JOURNAL OF AIRCRAFT
Vol. 46, No. 5, September–October 2009

# Numerical Investigation on Blade/Wake-Interaction Noise Generation

Y. Mauffrey,* G. Rahier, and J. Prieur
*ONERA, 92322 Chatillon, France*

DOI: 10.2514/1.32390

**This work investigates the potential of short-wave instability developing near blade tip vortex as the main source of blade/wake-interaction noise. In this aim, a numerical simulation of these instabilities is performed considering a simplified wake geometry. The aerodynamic fields are extracted to determine the blade pressure response using the unsteady compressible airfoil theory. Finally a loading-noise computation is performed. All the results obtained from these computations are compared with the experimental data and a good qualitative agreement is found.**

## Nomenclature

| | | |
|---|---|---|
| $A(k)$ | = | amplitude associated with wave vector **k** |
| $a$ | = | vortex core radius |
| $a_0$ | = | initial vortex core radius |
| $C$ | = | chord length |
| $c_z$ | = | lift coefficient |
| $d$ | = | separation distance between the two vortices |
| $f$ | = | chordwise pressure-jump distribution function |
| $E_k$ | = | kinetic energy associated with wave number $k$ |
| $k$ | = | axial wave number of the elliptic instability |
| **k** | = | wave vector associated with normal velocity perturbations |
| $M$ | = | Mach number |
| $md$ | = | distance between the blade and corotative vortex pair |
| $P$ | = | pressure |
| $P_{xc}$ | = | root-mean-square value as a function of normalized chord coordinates |
| $R$ | = | span |
| $(r, \theta, \varphi)$ | = | cylindrical coordinate system |
| $r_a$ | = | random number |
| $U_{av}$ | = | rotor advancing speed |
| $U_\infty$ | = | freestream velocity |
| $(u, v, w)$ | = | velocity field in the Cartesian coordinates system |
| $(u_0, v_0, w_0)$ | = | initial velocity field in the Cartesian coordinates system |
| $(v_r, v_\theta)$ | = | two-dimensional velocity field in the cylindrical coordinates system |
| $\beta$ | = | interaction angle between blade and corotative vortex pair |
| $\Gamma$ | = | circulation of the vortex |
| $\gamma$ | = | blade/vortex interaction angle |
| $\Delta c_p$ | = | pressure-jump coefficient |
| $\Delta p$ | = | local pressure jump across the airfoil |
| $\delta$ | = | vortex center displacement in the axial direction |
| $(\eta, \xi)$ | = | normalized Cartesian coordinates |
| $\lambda$ | = | instability wavelength |
| $\rho$ | = | density |
| $\sigma_k$ | = | instability growth rate associated with wave number $k$ |
| $\varphi$ | = | rotor azimuth |
| $\psi$ | = | angle between the span direction and the rotor forward-speed vector |
| $\boldsymbol{\Omega}$ | = | angular velocity of the rotor |
| $\Omega_0$ | = | vortex system angular velocity |

Received 28 May 2007; revision received 8 December 2008; accepted for publication 9 December 2008. 

*Research Scientist, Aerodynamics; yann.mauffrey@onera.fr.

## I. Introduction

BLADE/WAKE interaction (BWI) has been recognized as a significant component of main rotor noise, particularly in flight conditions such as climb or level flight, in which blade/vortex interaction (BVI) noise is less intense. In these flight conditions, BWI is a more important (or equivalent) source of noise in terms of intensity than BVI. Blade/wake interaction is characterized by broadband noise in a frequency domain between BVI noise and turboshaft engine noise (typically 1 to 3 KHz full scale).

This noise was initially identified by Brooks et al. [1]. Analyzing experimental acoustic spectra, he related BWI noise to nonperiodic blade pressure fluctuations in the midfrequency range. Brezillon et al. [2] established a relationship between these broadband pressure fluctuations and the blade wake by analyzing blade pressure measurements performed during the higher-harmonic-control aeroacoustic rotor test (HART) wind-tunnel test [3]. This work compared midfrequency blade pressure perturbation azimuthal occurrences on the rotor disk with close BVI events using a free-wake BVI prediction code. This comparison allowed us to associate BWI sources with perpendicular blade/vortex interactions. These interactions concern vortices under 180 deg of age. Glegg [4] built a BWI prediction model assuming that the noise results from the interaction between the blade and isotropic homogeneous turbulence contained in the tip vortices. His model indicated that the turbulent kinetic energy contained in an isolated vortex is not sufficient to account for BWI noise levels. This finding led Wittmer et al. [5] to look for alternative mechanisms of turbulence production within rectilinear vortices. Wittmer et al.'s work showed that the turbulent zones around vortices were larger when they had already interacted with a blade. Modifying their prediction model consequently, Glegg et al. [6] obtained BWI noise levels in agreement with experimental data. Contrary to the results of [4], analysis of experimental blade pressures in [2] showed that contributions to BWI noise from unperturbed tip vortices are comparable with those from vortices having encountered a blade.

A thorough analysis by Bouchet and Rahier [7] of the same HART experimental blade pressures, first studied in [2], demonstrated that BWI was not related to isotropic turbulence, but rather to the blade interactions with coherent large-scale structures present in the flow. Moreover, Bouchet and Rahier linked these structures to short-wave vortex instabilities. These instabilities occur when an external strain field deforms the vortex core elliptically. The deformation induces the resonant coupling of two vortex modes (Kelvin modes).

Observing that BWI pressure fluctuations occur at azimuths in which the blade interacts with two close tip vortices, Bouchet and Rahier [7] hypothesized that elliptic instabilities of corotating vortex

pairs are the source of BWI noise. Readers can refer to Le Dizes and Laporte [8] for a linear analytical study and Laporte and Corjon [9] for a numerical study of these instabilities. This paper aims at verifying, using numerical simulations, that short-wave instabilities developing near tip vortex cores can be a source of BWI noise. A climb flight condition is chosen. Because full-rotor computation is not presently feasible (the characteristic lengths of the instabilities' structures require a prohibitive number of points), it was chosen to adopt the alternative approach described subsequently.

First, the capability of the computational fluid dynamics (CFD) code elsA [10] to simulate the development of vortex elliptical instabilities is evaluated. Then a numerical simulation is performed for a pair of rectilinear, uniform, and parallel vortices on a limited domain.

The velocity perturbations issued from the computation are then used to determine the blade pressure fluctuations generated by the blade/vortex instability encounter. Amiet's theory [11] is employed to perform the prediction of the blade aerodynamic response to this perturbation field.

Eventually, these blade pressure perturbations are used as input data to a loading-noise computation performed using the PARIS [12] code. The acoustic computation is based on an integral formulation of the Ffowcs Williams and Hawkings equation solution.

Computed blade pressure perturbations and acoustic results are compared with the HART II [13] experimental data and discussed.

## II. Numerical Simulation of Short-Wave Instabilities

### A. Geometrical Characteristics of Tip Vortices

In this section, the geometrical characteristics of the problem is presented and the vortex short-wave instabilities that can be induced in this configuration are described.

Figure 1a shows tip vortices for a climb flight configuration. Particular attention should be given to the vortex conformation in the BWI occurrence zone ($\psi = 110$ deg). At this azimuth, a close interaction between the two tip vortices can be noted. This interaction could make possible the development of short-wave instabilities also called elliptic instabilities on each vortex. Figure 1b presents the harmonic analysis for the first branch of elliptical instability of a Lamb–Oseen-like vortex profile. The harmonic number is plotted as a function of the ratio $a/d$ (where $a$ is the vortex core size, and $d$ is the separation distance between the two vortices). This result is issued from the linear study of Le Dizes and Laporte [8]. It can be observed that the harmonic number of instabilities is in the frequency range of BWI centered about 250 times the rotor rotation frequency. It also appears that the ratio $a/d$ has a major influence on elliptical instabilities. The closer the vortices, the higher the instability growth rate and the larger the instability frequency range. The spatial extent of the instability also depends on this ratio. The instability originates near each vortex center and extends further to its periphery as the ratio $a/d$ increases. The latter phenomenon is caused by the saturation of the short-wave instability at small amplitudes and small $a/d$ ratios.

Thus, an estimation of $a/d$ is needed to pursue the discussion on the type of instabilities that can occur. A free-wake computation together with a physical model of the core size evolution was employed for this purpose. With this method, an average ratio of $a/d = 0.10$ was obtained in the main azimuthal range of BWI (90–120 deg). This ratio appears to be in a middle range and is sufficient to spawn elliptical instabilities that thus appear as a possible BWI noise source. It should also be noted that the medium value of $a/d$ implies that the instability remains confined in the vortex vicinity. As a consequence, one can consider the evolution of the instability to occurr on one vortex independently from the other.

More generally, short-wave instabilities can occur when a vortex experiences an external strain field that elliptically deforms its core. The strain field induced by the rotor wake on the tip vortices could thus also be a source of instability. This could explain the experimental pressure fluctuations associated with BWI appearing at azimuths in which the distance between the vortices is larger.

### B. Numerical Simulation

An Euler numerical simulation is performed. Viscosity is assumed to have a weak influence in the first steps of the instability development. The numerical tool used to simulate the two-dimensional and three-dimensional dynamics of the two vortex flows is the ONERA finite volume Navier–Stokes solver elsA [10]. This solver uses structured meshes. The simulations are performed using a fourth-order explicit Runge–Kutta scheme for time integration. A second-order Jameson skew-symmetric centered scheme is used for the advection terms. No second-order dissipation is imposed and the fourth-order dissipation term is set to have minimum diffusion. Periodic boundary conditions are applied on the domain edges cutting the vortices, and far-field conditions are applied on the other domain boundaries.

The mesh is locally refined in the crossflow plane in the region of the two vortices to reach 10 points in the vortex core radius. Laporte and Corjon [9] showed that this discretization is enough to simulate the elliptical vortex core deformation. In this direction, the boundaries are far from the vortex pair (the distance between the center of the domain and boundaries is of the order of 10 times the initial vortex separation distance). The total number of points is 47,961 in the crossflow plane. A comparison of the computed instability growth rate with the theoretical ones obtained by Le Dizes and Laporte [8] from linear analysis, the mesh size in the axial direction is set equal to the wavelength that has to be simulated. A distribution of 20 points per wavelength is chosen in this direction.

The flow is composed of a pair of parallel rectilinear and uniform corotating vortices centered in the crossflow direction of the computational domain. The circulations of the two vortices are identical. A Lamb–Oseen-like vortex velocity profile is chosen. In a cylindrical

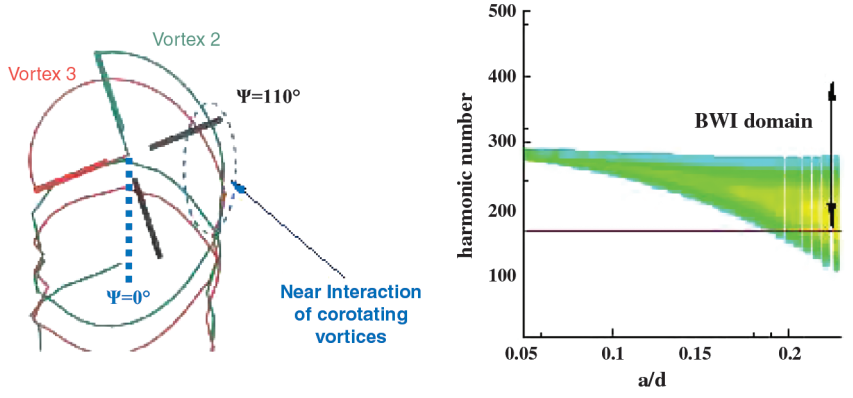


a) b)

**Fig. 1 Illustrations of a) rotor tip vortices during a climb flight and b) harmonic analysis of short-wave instabilities versus $a/d$. Color scale: the instability growth rate increases from green to yellow.**

coordinate system, the definitions of velocity and pressure relative to this profile are

$$\begin{cases} v_r = 0 \\ v_\theta = \frac{\Gamma}{2\pi r}\left(1 - e^{\frac{r^2}{a_0^2}}\right) \\ \frac{\partial P}{\partial r} = \rho \frac{v_\theta^2}{r} \end{cases} \quad (1)$$

This tangential velocity profile $v_\theta$ has been compared by Han et al. [14] with experimental laser Doppler velocimetry measurements and has been found to be an acceptable approximation. No experimental results were found in literature about axial velocity profile at climb flight conditions. Experimental results of McAlister [15] and Han et al. [14] from particle image velocimetry and laser Doppler velocimetry measurements on a hovering rotor gave a ratio between maximum tangential velocity and axial velocity greater than 5. Laporte and Corjon [9] showed that for this ratio, the axial velocity has a weak influence on the instability modes developing inside the vortices. Moreover, the axial velocity does not play a dominant part in the determination of the acoustic sources. Consequently, the axial velocity deficit is not taken into account. The three-dimensional computation is set as follows:

1) Initial conditions are given by a preliminary 2-D computation. The linear superposition of the two Lamb–Oseen vortices' aerodynamic fields is not the solution of Euler equations. This fact could introduce an error in the 3-D instability computation. Indeed, the linear superposition is introduced as the initial condition of a 2-D computation. During the simulation, the strain field induced by one vortex on the other elliptically deforms the other vortex core, and the vortex system begins to rotate at an angular velocity $\mathbf{\Omega}_0 = (0, 0, \Gamma/2\pi d^2)$. This simulation is performed until a converged solution is reached.

2) The aerodynamic solution obtained is then introduced, extending the velocity, pressure, and density fields to the third dimension and perturbing the velocity fields by white noise. If $(u_0, v_0, w_0)$ is the unperturbed velocity field at each mesh point, the white noise is introduced as follows: let $r_a$ be a random number in the range of $-0.5 \times 10^{-3}$ to $0.5 \times 10^{-3}$; thus,

$$\begin{cases} u = u_0(1 + r_a) \\ v = v_0(1 + r_a) \\ w = 0 \end{cases} \quad (2)$$

In the following, only the results until the start of the nonlinear amplification regime will be taken into account.

### C. Results

Three-dimensional elliptic instability results in a sinusoidal deformation in the vortex axial direction. Le Dizes and Laporte [8], in the context of linear instability theory, gave an analytical approximation of the instability growth rate as a function of the vortex-pair characteristics. To evaluate the elsA aerodynamic code's ability to simulate the development of the instability, a series of computations were carried out, focused on a wavelength. The circulation $\Gamma$ and the initial viscous core radius $a_0$ were deduced from results of the ONERA BVI computation chain [16]. For the HART II mild climb flight condition, we found $\Gamma = 4.7\ \mathrm{m}^2 \cdot \mathrm{s}^{-1}$ and $a_0 = 0.0168$ m. The instability development inside vortices is presented subsequently.

1) A linear amplification phase in which kinetic energy $E_k$, associated with only one wavelength, exponentially grows as $E_k(t) = E_k(0)e^{\sigma_k t}$, where $t$ denotes the time and $\sigma_k$ is the growth rate.

2) Then a weakly nonlinear regime of instability development appears, meaning that subharmonics of the fundamental mode are amplified.

3) At last, a nonlinear regime occurs. This regime corresponds to the amplification of all the computed modes. In our study, due to the small value of $a/d$, a nonlinear saturation of the instability at short amplitudes is observed. Sipp [17], in the context of weakly nonlinear analysis of contrarotating vortex-pair instability, has shown that the amplitude of instability saturation increases with the ratio $a/d$. In our case, if $\delta$ is the vortex center displacement in the axial direction (located at the vorticity maximum), the ratio $\delta/d = 0.0097 \pm 0.00175$ is obtained. This result is in quite good agreement with Sipp's predictions.

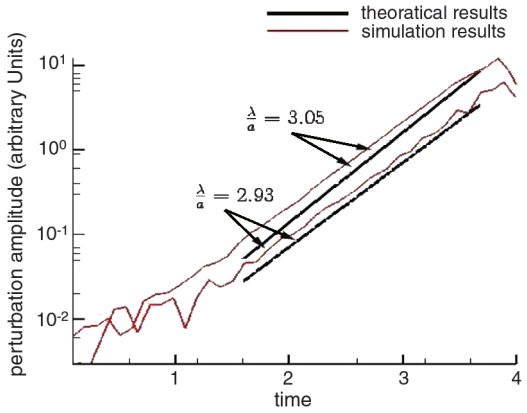


**Fig. 2 Theoretical and present numerical simulation comparison of the time-amplification mode in the linear regime of elliptic instability. (Time is normalized by the rotor revolution period.)**

Figure 2 shows the comparison between theoretical evolution of the amplified mode predicted by Le Dizes and Laporte [8] and the evolution of kinetic energy perturbation related to the amplified mode in linear regime found by the present simulation for two different values of wavelength $\lambda = 2\pi/k$. The evolution of the amplitude of the instability mode is obtained by the following procedure. At each time step of the simulation, the instantaneous kinetic energy associated with a single vortex is averaged over each orthoaxial plane of the simulation domain. A kinetic energy according to the axial direction of the vortex is thus obtained. The square root of this kinetic energy is then decomposed into axial Fourier modes. Finally, the growth rate of the instability is obtained from the time evolution of the most amplified mode.

Note in Fig. 2 that the growth rates obtained from the simulations are close to those predicted by Le Dizes and Laporte [8]. A difference of 7% on the normalized wavelength $\lambda/a = 3.05$ and less than 2% on $\lambda/a = 2.93$ is observed. One can see that the time necessary for the instability development does not correspond to the hypothesis of an interaction of the blade with vortices "younger" than 180 deg. This disagreement could be due to the fact that, contrary to the numerically simulated configuration, actual tip vortices are neither rectilinear nor parallel. Moreover, tip vortex velocity profiles are not axisymmetric as assumed in the vortex analytical model here. A study of the frequency range and growth rate of the instability in a more realistic configuration will remain for a future work. Nevertheless, this simulation computed with a simplified configuration allows a first analysis of the phenomenon and potential sources of noise that blade/vortex instability interaction can generate. This acoustic aspect is developed in the following section.

## III. Acoustic Analysis

In this section, the acoustic consequences of perpendicular interaction between perturbed vortices and a rotor blade in the context of helicopter rotor flow is evaluated. With this goal, the pressure fluctuations that normal perturbations of the velocity field would generate on a blade are computed. This is achieved by extracting information from a selected plane of the 3-D CFD computation and evaluating the pressure-jump perturbation on the blade based on Amiet's [11] compressible gust/airfoil theory. Then a loading-noise prediction is performed starting from these pressure-jump time histories.

### A. Determination of the Gust

The numerical simulation of elliptic instabilities is worked out on a mesh that allows amplification of several axial wavelengths. The

axial extent of the domain corresponds to 2.1 chords. Figure 3 shows isocontours of vorticity for different stages of the instability development. Figure 3a shows the linear stage of instability, Fig. 3b shows the final amplitude of the axial wavelength at the end of the linear instability phase, Fig. 3c shows the vortex deformation in the late stage of the weakly nonlinear phase, and Fig. 3d the nonlinear saturation of the perturbed vortex.

To determine the blade pressure fluctuations, a 2-D plane is extracted from the 3-D CFD computation domain. Only the normal component of the velocity field with respect to this plane is considered. Presently, Amiet's [11] theory enables us to compute the aerodynamic response of a flat-plate airfoil to this two-dimensional gust (see Fig. 4b). The 2-D plane is extracted considering a constant interaction angle $\beta$ and constant distance $md$ between the blade and the corotating vortex pair (see Fig. 4a). The extent of the extracted plane in the spanwise direction corresponds to 5% of the blade span.

### B. Blade Pressure Fluctuations

To determine the pressure perturbations resulting from the incident velocity perturbation that the blade would experience when passing next to the perturbed vortex, Amiet's [11] theory is used. One considers that the gust obtained by the procedure presented before is carried by a freestream velocity $U_\infty = \Omega R + U_{av}\sin(\psi)$, where $\Omega$ is the angular velocity of the rotor, $R$ is the normalized span coordinate, $U_{av}$ is the rotor advancing speed, and $\psi$ is the angle between the span direction and the forward-speed vector. In this approach, the spanwise position and the interaction angle $\gamma$ between the blade and the vortex axis are taken into account. Values of $\gamma$, $\beta$, and $md$ are deduced from [16]. In the following, the $\eta$ axis is oriented in the chordwise direction, and $\xi$ is oriented in the spanwise direction. Both of these coordinates are normalized by the half-chord $C/2$, so that $\eta$ ranges between $-1$ and 1 and $\xi$ between $-A$ and $A$.

For a normal velocity perturbation of wave-number vector $\mathbf{k} = (k_\eta, k_\xi)$ [with $k_\eta = (2k/C)\cos(\gamma)$ and $k_\xi = (2k/C)\sin(\gamma)$], assuming that freestream angle of attack is null, Amiet [18] defined the local pressure jump $\Delta P$ across the airfoil as

$$\Delta P(\mathbf{k}, t, \eta, \xi) = \pi\rho U_\infty A(\mathbf{k}) g(\eta, \mathbf{k}, M) e^{i(k_\xi \xi - k_\eta U_\infty / C)t} \tag{3}$$

where $A(\mathbf{k})$ is the amplitude associated with the wave-number vector $\mathbf{k}$, $M$ is the Mach number, $\rho$ is the density, and $g$ is the local transfer function between incident velocity and airfoil pressure jump. The lift coefficients are obtained by integrating the pressure forces over the chord and summing the contributions of all wave numbers:

$$c_z(t, \xi) = \frac{2}{\rho(U_\infty C/2)^2} \int_{-\infty}^{+\infty} \int_{-1}^{1} \Delta P(\mathbf{k}, t, \eta, \xi)\, \mathrm{d}\eta\, \mathrm{d}\mathbf{k} \tag{4}$$

For high frequencies, if the gust/airfoil intersection moves supersonically relatively to the fluid, the airfoil response function has been given by Amiet [18] as

$$g(\eta, \mathbf{k}, M) = g_1(\eta, \mathbf{k}, M) \times \left(1 + \frac{\sqrt{1+\eta}}{2}\left[(1+i)E\left(2\frac{k_\eta}{1-M^2} M_\infty (1-\eta) - 1\right)\right]\right) \tag{5}$$

With

$$M_\infty = \sqrt{M^2 - (1-M^2)\frac{k_\eta^2}{k_\xi^2}}$$

and

$$E(x) = \frac{1}{\sqrt{2\pi}} \int_0^x \frac{e^{-it}}{\sqrt{t}}\, \mathrm{d}t$$

$g_1$ is defined as

$$g_1(\eta, \mathbf{k}, M) = \frac{1}{\pi\sqrt{\pi(1+M)k_\eta(1+\eta)}} e^{-i\frac{k_\eta}{1-M^2}(M_\infty(1+\eta) - M^2\eta - 1) + \pi/4} \tag{6}$$

#### 1. Chordwise Signal Characteristics

Burley et al. [19] examined the experimental pressure-jump spectra of the HART I test for different chordwise sensor locations in the azimuthal domain in which BWI occurs. They noted that the falloff in spectral response was similar for all the $\eta$ values. This property tends to show that chordwise pressure distribution can be expressed solely as a function of this variable and is independent of the gust wave number. Thus, it seems that the chordwise pressure distribution proposed by Amiet [18] in Eq. (3) is not suited for this case. Indeed, Amiet's [11]theory assumes that the distribution of pressure perturbations in the chordwise direction depends on the considered wave number. For this reason, in the following, only the section lift coefficient obtained by Amiet's theory is considered.

Nevertheless, when considering a high-frequency gust encountering an airfoil, it is well known that a compact chordwise approximation is not well suited for acoustic simulations. For this reason, a chordwise pressure distribution function, denoted by $f$, has been designed to distribute the lift coefficient, predicted by Amiet's [11] theory, along the blade chord. A continuous and integrable function, for which the shape is similar to the stationary pressure-jump distribution, is desired. This function thus gives more importance to the lift near the leading edge and then decreases as $\eta$ increases. The decrease of the function $f$ has been evaluated from densely instrumented blade sections of the experimental HART II data. An example of experimental signal from HART II corresponding to pressure for the blade section $\xi C/2 = 0.87R$ at 3 and 6% chord transducer locations is provided in Fig. 5. The figure shows high-variance pressure fluctuations related to the two oblique blade/vortex interactions with vortex 2 and vortex 3 defined in Fig. 1.

The rms value $P_{(\eta-1)/2}$ of this signal is then evaluated in each azimuthal window corresponding to interactions. For example,

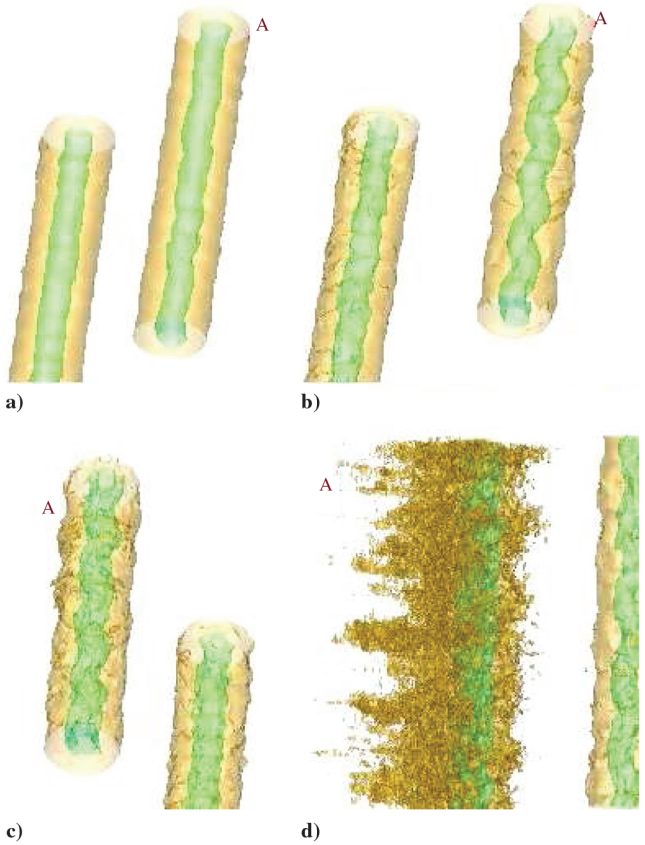


**Fig. 3 Isovorticity contours in different regimes of the elliptic instability for vortex A: a) first stage of the linear regime, b) end of the linear regime, c) weakly nonlinear regime, and d) nonlinear saturation.**

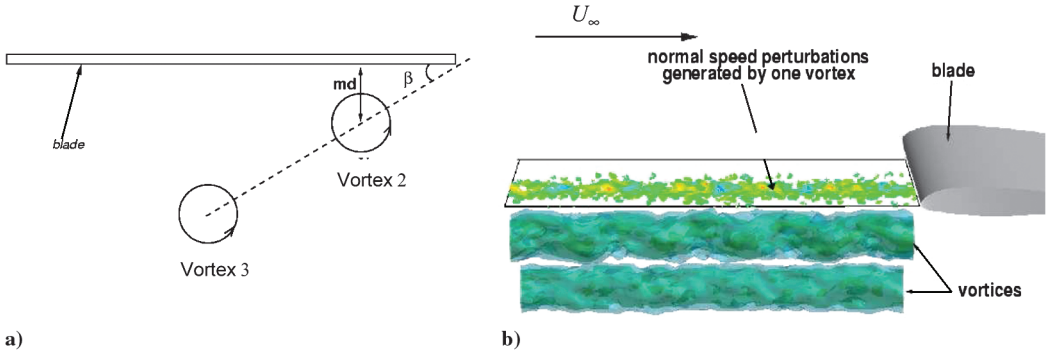


**Fig. 4 Illustrations of a) schematic representation of blade/vortex-pair interaction and b) example of extracted gust plane.**

considering the windows associated with the blade/vortex 2 interaction result gives ratios $P_{0.06}/P_{0.03} = 0.48$ and $P_{0.1}/P_{0.03} = 0.35$. The results are similar for the window associated with vortex 3. The chordwise pressure-jump distribution function $f$ is deduced from this information:

$$f(\eta) = \frac{2}{I_f}\frac{1 - e^{(-\alpha(\eta+1)^2/(2(0.02)^2)}}{1+\eta} \tag{7}$$

where $\alpha = \sqrt{1.256}$ is a constant adjusted to obtain a maximum value of $f$ for $\eta = -0.96$, and $I_f$ is the value of the integral of $f$ over the chord. Consequently, the pressure-jump coefficient will be distributed over the chord as follows:

$$\Delta c_p(\eta) = c_z f(\eta) \tag{8}$$

where $c_z$ is the section lift coefficient.

### 2. *Spanwise Signal Characteristics*

Spanwise pressure-jump correlation will have a major influence in the property of the radiated noise. Indeed, it will drive the noise intensity and directivity; the radiated noise becomes more directive and more intense as the spanwise correlation length increases. Using the HART II data, the spanwise pressure-jump correlation associated with BWI noise has been evaluated by considering the instantaneous data for a rotor period and subtracting from it by the mean pressure data (i.e., pressure-jump time history for a selected rotation minus ensemble-averaged data on 100 rotations).

For a climb flight condition, the pressure perturbations associated with BWI in the azimuthal range of $90\,\text{deg} < \psi < 120\,\text{deg}$ are localized in the spanwise domain ($0.85R$:$0.94R$). The results, presented in Figs. 6 and 7, show that the pressure jumps are well correlated for a spanwise extent of 1 and 2% rotor span.

Figure 8 shows an example of instantaneous pressure-jump perturbation evolution in the spanwise direction obtained from blade pressure computations. Only the pressure jumps above 200 Pa are considered. This threshold value represents the order of magnitude of random fluctuations of the pressure signal (not related to BWI) deduced from experimental data. Considering this assumption, the results found here gave a spanwise extent of about 2% of the blade span.

## C. Results

In this section, the procedure used to compute the blade pressure jump is described. The results of noise loading computations performed using the compact chordwise approximation and the chordwise distributed sources are then compared.

In the following, two different interactions of the blade with perturbed vortices is considered. The relative interaction configurations are deduced from the wake geometry presented in Fig. 1. The gust is extracted from the numerical simulation at a time corresponding to the end of the linear regime (Fig. 3b). The vortex axial deformation due to the elliptical instability develops in a preferential plane. This phenomenon suggests that the geometrical parameters such as angle $\beta$ have a major influence in the computation of blade response. In our study, a free-wake computation is used to determine $\beta$. Thus, this angle will not be adjusted to obtain maximum pressure-jump amplitude. The azimuthal range $D$ on which pressure-jump fluctuations will be imposed is $D = 90$ to 120 deg. $\beta$ has been set as the average angle value obtained from the wake computation in the azimuthal domain $D$. A value of $\beta = 7\,\text{deg}$ is found. The constant distance $md$ related to the blade/vortex 2 distance is set to $md = 0.16C$. Finally, the gust/airfoil angle of interaction is set to 10 deg for vortex 2 and 15 deg for vortex 3.

Figure 9 presents the time history of the computed pressure-jump fluctuations at the spanwise coordinate $\xi C/2 = 0.87R$. The pressure-jump perturbations are obtained from Amiet's [18] lift coefficient distributed along the chord according to the function $f$. The first 100 harmonics have been removed. The amplitudes of the fluctuations associated with vortex 2 are weaker than those obtained from the

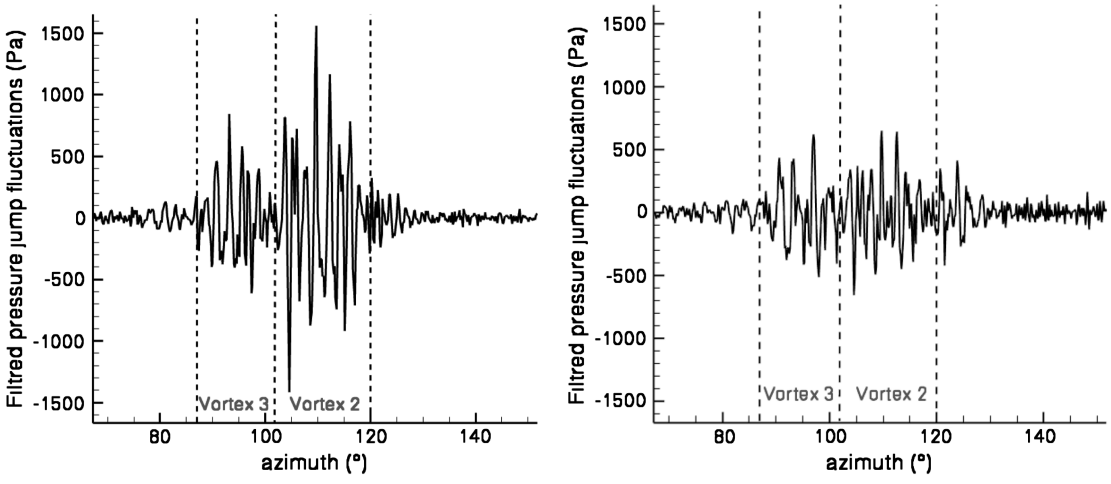


**Fig. 5 Typical experimental high-pass-filtered blade pressure jump as a function of azimuth for $\xi C/2 = 0.87R$; 3% chord (left) and 6% chord (right).**

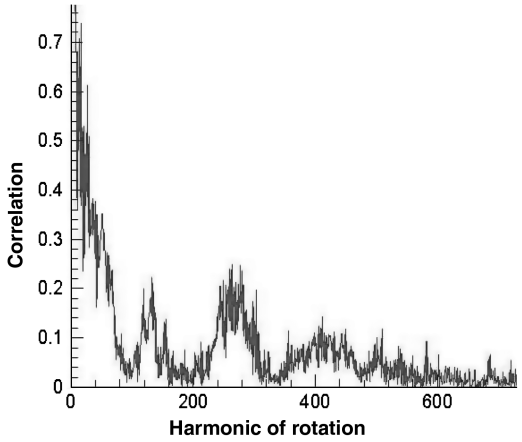


**Fig. 6 Spanwise pressure-jump correlation between two sensors: $0.87R$ and $0.88R$.**

experimental data presented in Fig. 5. Note that the azimuthal domain of the pressure fluctuations associated with vortex 2 is similar to the one observed in the experiment. However, the azimuthal domain of the pressure fluctuations associated with vortex 3 is smaller. This point could be explained by the hypothesis of constant angle of interaction $\gamma$. Also, unlike what has been observed in the experimental data, the average pressure fluctuation amplitude

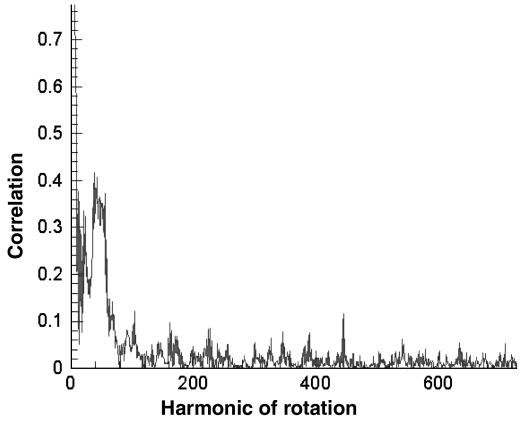


**Fig. 7 Spanwise pressure-jump correlation between two sensors: $0.85R$ and $0.87R$.**

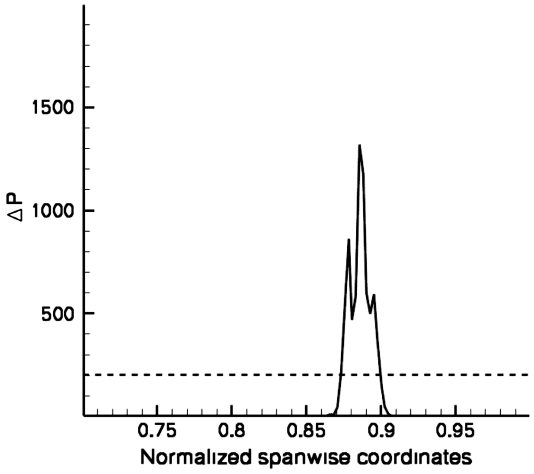


**Fig. 8 Representative computed spanwise distribution of pressure-jump perturbation.**

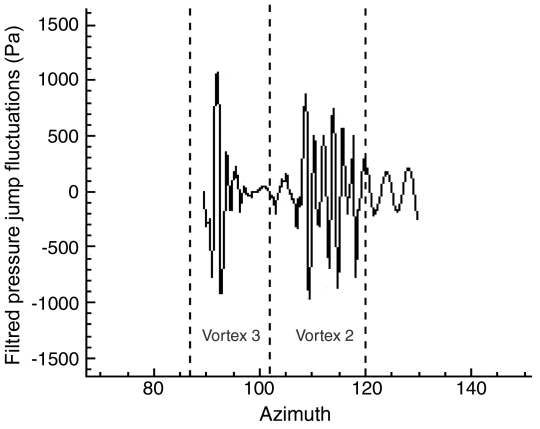


**Fig. 9 Blade/vortex interaction pressure-jump fluctuations computed $\xi C/2 = 0.87R$.**

associated with blade/vortex 3 interaction is more intense than the average pressure fluctuation amplitude of blade/vortex 2 interaction. This can be explained by the fact that distances between the blade and the vortices are roughly equal in our computations, whereas the experiment suggests a larger distance between the blade and vortex 3 than with vortex 2.

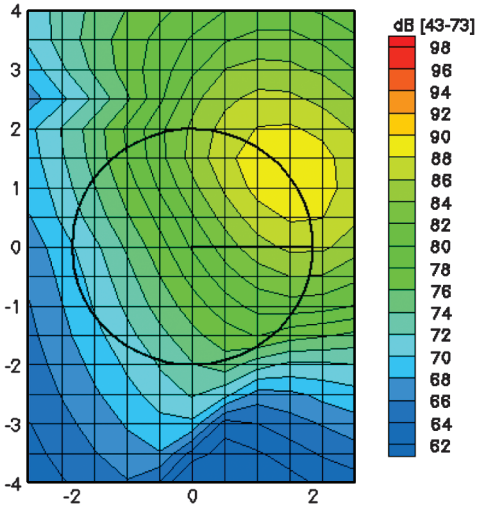


**Fig. 10 Computed noise footprint related to blade/vortex 2 interaction obtained with compact chordwise approximation.**

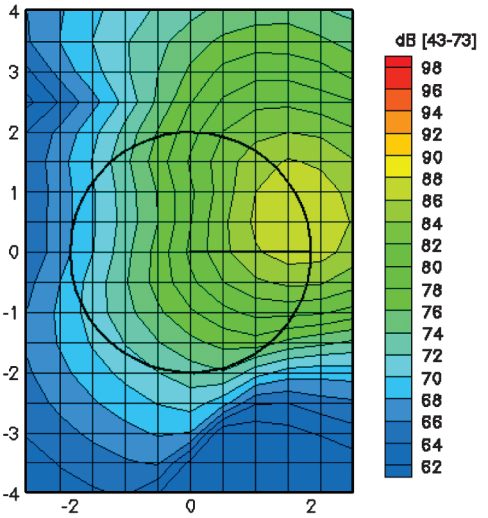


**Fig. 11 Computed noise footprint related to blade/vortex 2 interaction obtained from distribution of the lift.**

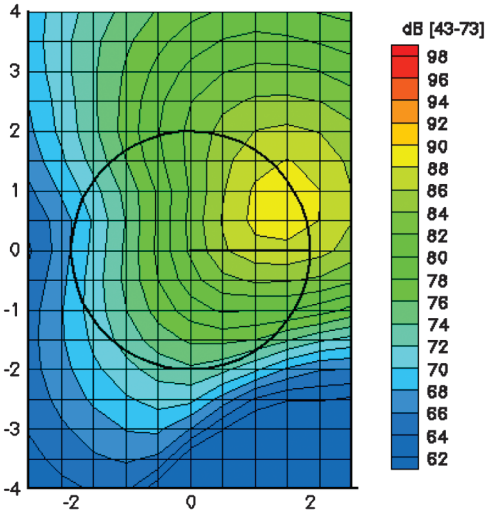


**Fig. 12 Computed noise footprint related to blade/vortex 3 interaction obtained from distribution of the lift.**

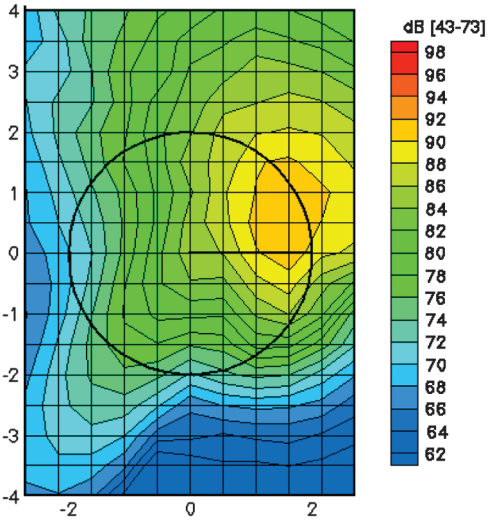


**Fig. 13 Noise footprint related to blade/vortex 2 and blade/vortex 3 interactions obtained from distribution of the lift.**

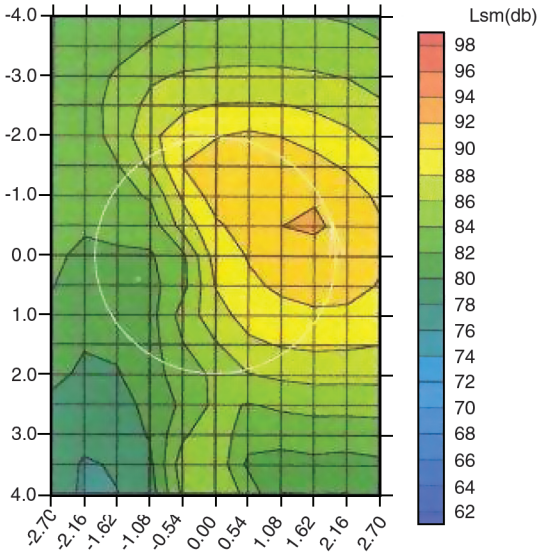


**Fig. 14 Experimental noise contours of BWI for a climb flight configuration. (Average spectrum filtered between 3 and 6.5 Khz.)**

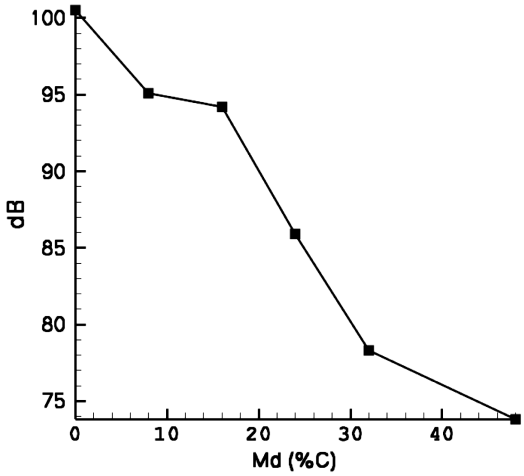


**Fig. 15 Maximum-noise-level evolution as a function of blade/vortex interaction distance *md*.**

Figures 10–13 show predicted noise footprints using PARIS from different computations. The microphone layout is situated in a horizontal plane at 1.2 rotor radius under the rotor. Noise levels are expressed in decibels filtered between 43 and 73 in blade passage frequency. Figures 10 and 11 show the noise footprint associated with blade interaction with vortex 2. Figure 10 is issued from a computation performed with compact chordwise approximation, and Fig. 11 is from a computation using distributed sources in the chordwise direction. As expected, compact chordwise approximation has an influence on both the directivity and the noise level. Indeed, the maximum noise zone is situated upstream of the rotor disk when considering compact sources and is situated on the right of the rotor disk when considering distributed sources. Moreover, maximum noise level is higher in the case of computation from compact sources (89.7 dB) than with distributed sources (87.7 dB).

Figure 12 shows the noise footprint associated with blade interaction with vortex 3 using a chordwise distributed source. A maximum noise level of 89.1 dB is noted, and a maximum noise zone is located more inboard of the rotor disk than in the case of interaction with vortex 2.

Finally, Fig. 13 presents the noise footprint obtained from a computation in which the interactions between the blade and both the vortices are considered. The relative good agreement in noise level between experiment (presented in Fig. 14) and our computation may be considered fortuitous in regard to the lack of accuracy in the determination of interaction parameters. What makes mores sense, however, is the good agreement in directivity between computation and experiment.

To illustrate the influence of the geometrical parameters, Fig. 15 shows the predicted maximum noise level for different values of the vortex-pair distance from the blade *md*. Note that the noise level decreases rapidly as the distance increases. This parameter *md*, as well as $\beta$, only has an influence on the noise level. The angle between the blade and the interacting vortex axis $\gamma$ has a weak influence on the noise directivity.

## IV. Conclusions

A CFD simulation of short-wave instabilities that may occur inside helicopter rotor tip vortices has been performed for the climb flight conditions in a simplified configuration of two analytical parallel rectilinear vortices. The instability mechanisms have been described and the influence of the parameters driving the instability growth rate has been discussed. A good agreement has been observed between numerical and theoretical linear growth rate.

Then the unsteady aerodynamic field provided by the numerical simulation has been used to compute the surface pressure response of rotor blades during a close encounter with such vortex instabilities in conditions in which BWI noise occurs. For this, a 2-D gust has been

extracted from the CFD computation and the blade response has been deduced from compressible Amiet's [11] theory. Comparable amplitudes have been observed between computed blade pressure fluctuations and corresponding HART II experimental results.

In the last part of the paper, these blade pressure fluctuations are used as input data for a loading-noise computation. The noise levels and directivity in a horizontal plane below the rotor are computed and compared with HART II experimental data. A good agreement in terms of noise levels and directivity is observed.

The results tend to show that interaction between rotor blades and vortices subject to elliptical instabilities is a good candidate mechanism to explain BWI generation. This supports the hypothesis laid by Bouchet and Rahier [7].

Nevertheless, our study presents some uncertainties that should be removed in the future. As shown in this paper, elliptical instabilities expand in a preferential direction and their growth rate depends on the distance separating the two vortices. Thus, the geometrical arrangement of the wake has a major importance in the instability development. The effect of a more realistic configuration (pair of nonparallel and nonuniform vortices) on the expansion of this kind of short-wave instabilities will be studied. Furthermore, because blade/vortex interaction parameters such as $md$ and $\beta$ are key parameters for noise production, a finer description of the wake is needed. It could be provided in the future, due to CFD progress.

## Acknowledgment

The authors would like to acknowledge Guillaume Perez for his participation in this study.

## References

[1] Brooks, T. F., Jolly, J. R., and Marcolini, M. A., "Helicopter Main-Rotor Noise: Determination of Source Contributions Using Scaled Model Data," NASA TP 2825, Aug. 1988.

[2] Brezillon, J., Prieur, J., and Rahier, G., "Investigation on Broadband Helicopter Rotor Noise," *AHS Rotorcraft Acoustics and Aerodynamics Specialists Meeting*, AHS International, Alexandria, VA, Oct. 1997.

[3] Splettstoesser, W. R., Kube, R., Wagner, W., Seelhorst, U., Boutier, A., Micheli, F., Mercker, E., and Pengel, K., "Key Results from a Higher Harmonic Control Aeroacoustic Rotor Test (HART)," *Journal of the American Helicopter Society*, Vol. 42, No. 1, 1997.

[4] Glegg, S. A. L., "The Prediction of Blade Wake Interaction Noise Based on a Turbulent Vortex Model," 12th AIAA Aero-Acoustics Conference, San Antonio, TX, AIAA Paper 1134, 1989.

[5] Wittmer, K. S., Devenport, W. J., and Glegg, S. A. L., "Perpendicular Blade Vortex Interaction," *AIAA Journal*, Vol. 33, No. 9, Sept. 1995, pp. 1667–1674.
doi:10.2514/3.12802

[6] Glegg,, S. A. L., Witmmer, S., Devenport, S., and Pope, D. S., "Broadband Helicopter Noise," *AHS Specialists' Meeting for Rotorcraft Acoustic and Aerodynamics*, AHS International, Alexandria, VA, Oct. 1997.

[7] Bouchet, E., and Rahier, G., "Structure of the Blade Pressure Fluctuations Generated by Helicopter Rotor Blade-Wake Interaction," *56th American Helicopter Society Annual Forum*, AHS International, Alexandria, VA, May 2000.

[8] Le Dizes, S., and Laporte, F., "Theoretical Predictions for Elliptical Instability in a Two Vortex Flow," *Journal of Fluid Mechanics*, Vol. 471, Nov. 2000, pp. 169–201.

[9] Laporte, F., and Corjon, A., "Direct Numerical Simulations of the Elliptic Instability of a Vortex Pair," *Physics of Fluids*, Vol. 12, May 2000, pp. 1016–1031.
doi:10.1063/1.870357

[10] Gazaix, M., Jolles, A., and Lazareff, M., "The elsA Object-Oriented Computational Tool for Industrials Applications," *23rd Congress of ICAS* [CD-ROM], Toronto, Canada, International Council of the Aeronautical Sciences, Sept. 2002.

[11] Amiet, R. K., "High Frequency Thin-Airfoil Theory for Subsonic Flow," *AIAA Journal*, Vol. 14, No. 8, 1976, pp. 1076–1082.
doi:10.2514/3.7187

[12] Beaumier, P., and Spiegel, P., "Validation of ONERA Aeroacoustic Prediction Methods for Blade-Vortex Interaction Using HART Tests Results," *American Helicopter Society 51st Annual Forum*, AHS International, Alexandria, VA, May 1995.

[13] Van der Wall, B., Junker, B., Raffel, M., Richard, H., Wagner, W., Burley, C. L., Brooks, T. F., Yu, Y. H., Tung, C., Mercker, E., Pengel, K., Holthusen, H., Beaumier, P., and Delrieux, Y., "The HART-II Test in the LLF of DNW—A Major Step Towards Rotor Wake Understanding," 28th European Rotorcraft Forum, Royal Aeronautical Society Paper 42, Sept. 2002.

[14] Han, Y. O., Leishman, J. G., and Coyne, A. J., "On the Turbulent Structure of a Tip Vortex Generated by a Rotor," *52th American Helicopter Society Annual Forum*, AHS International, Alexandria, VA, 4–6 June 1996.

[15] McAlister, K. W., "Rotor Wake Development During the First Revolution," *59th American Helicopter Society Annual Forum*, AHS International, Alexandria, VA, 6–8 May 2003.

[16] Rahier, G., and Delrieux, Y., "Blade Vortex Interaction Noise Prediction Using a Rotor Wake Roll-Up Model," *Journal of Aircraft*, Vol. 34, No. 4, 1997, pp. 29–41.

[17] Sipp, D., "Weakly Nonlinear Saturation of Short Wave Instabilities in a Strained Lamb-Oseen Vortex," *Physics of Fluids*, Vol. 12, No. 7, 2000, pp. 1715–1729.
doi:10.1063/1.870422

[18] Amiet, R. K., "Noise Produced by Turbulent Flow into a Rotor: Theory Manual for Noise Calculation," NASA CR-181788, 1989.

[19] Burley, C. L., Brooks, T. F., Splettstoesser, W. R., Schultz, K.-J., Kube, R., and Bucholtz, H., "Blade-Wake Interaction Noise for a BO-105 Model Main Rotor," *AHS Specialists' Meeting for Rotorcraft Acoustic and Aerodynamics*, AHS International, Alexandria, VA, Oct. 1997.